H. KRAWIEC*#, V. VIGNAL**, M. LATKIEWICZ*,**

MICROSTRUCTURE AND CORROSION BEHAVIOUR OF Co-Mo/TiO$_2$ NANO-COMPOSITE COATINGS FORMED ON DISK AND WIRE ELECTRODES BY ELECTRODEPOSITION

The influence of the electrode geometry on the microstructure and corrosion behaviour of Co-Mo nano-crystalline coatings elaborated by electrodeposition is studied. The corrosion behaviour was determined in the Ringer's solution at 25°C. Electrodeposition mechanisms are also discussed as a function of the electrode geometry. The electrode geometry was found to affect the growth rate and, under certain conditions, the microstructure (existence of channels and pores). It does not have influence on the corrosion behaviour.

Keywords: cobalt, molybdenum, nano-crystalline coating, corrosion, dissolved oxygen

1. Introduction

Co-Mo/TiO$_2$ nano-composite coatings can be electrodeposited on metallic alloys. Previous work [1] has shown that the level of residual stress in these coatings remains low during electrodeposition. Thick and compact (crack-free) coatings can then be elaborated. They have also good adhesion. In addition, these coatings may have the same physical-chemical properties than Co-Mo nano-crystalline coatings which have high hardness, high thermal resistance and good magnetic properties [2-15].

The microstructure of Co-Mo/TiO$_2$ nano-composite coatings has already been investigated for different electrodeposition times [1]. A growth mechanism model based on the local diffusion field has recently been proposed for long-term electrodeposition [16]. The corrosion behaviour has been studied after long-term immersion in NaCl-based media [1] and after tribological and scratch tests [17]. Co-Mo/TiO$_2$ nano-composite coatings exhibit good tribological properties.

In the present paper, the influence on the electrode geometry on electrodeposition mechanisms was first studied. The microstructure of coatings electrodeposited on disk and clamped wire electrodes was then compared. The corrosion behaviour in NaCl media was also determined for the two types of electrodes.

2. Materials, and Methods

2.1. Materials and surface preparation

The substrate was made of ultra-pure Co (Co: 99.99 + wt%, Al < 1 ppm, Ag < 2 ppm, Cr < 1 ppm, Cu < 3 ppm, Fe < 7 ppm, Mg < 1 ppm and Si < 5 ppm). It was delivered by Goodfellow in the form of as drawn rods (diameter of 1.2 cm) and wires (diameter of 100 µm). Rods were cut and embedded in an epoxy resin (surface area of 1.13 cm^2, Fig. 1(a)). They were then mechanically ground with emery papers (down to 4000 grit), cleaned in ethanol under ultrasonics for 5 minutes and dried in air. Wires were cut and clamped in a home-made system (Fig. 1(b)), cleaned in ethanol under ultrasonics for 5 minutes and dried in
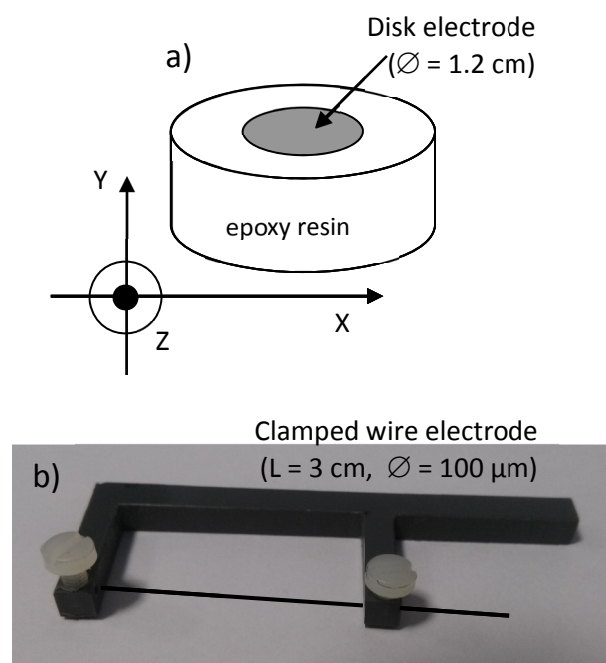

Fig. 1. Electrodes used for electrodeposition: (a) disk electrode and (b) clamped wire electrode

*   AGH-UNIVERSITY OF SCIENCE AND TECHNOLOGY, FACULTY OF FOUNDRY ENGINEERING, REYMONTA 23 STR., 30-059 KRAKOW, POLAND
**   ICB UMR 6303 CNRS – UNIVERSITÉ BOURGOGNE FRANCHE-COMTÉ, DIJON, FRANCE

Corresponding author: krawiec@agh.edu.pl

24

air. The body of this home-made system was entirely made of PVC (chemically inert and rigid) and the wires were made of nylon (chemically inert and rigid).

Co-Mo/TiO$_2$ nano-composite coatings were electrodeposited on disk electrodes (corresponding to embedded rods) and on clamped wire electrodes under the same experimental conditions. The potential was set at -1.2 V vs. SCE for different times (between 5 minutes and 250 minutes). The aqueous solution (volume of 150 mL) was composed of 0.2M CoSO$_4$ 7H$_2$O + 0.02M Na$_2$MoO$_4$ 2H$_2$O + 0.5M H$_3$BO$_3$ + 0.3M Na$_3$C$_6$H$_5$O$_7$ + 20 g/L TiO$_2$ (primary particle size of 21 nm, provided by Sigma-Aldrich). It was stirred using a magnetic stirrer (260 rpm). The solution pH and temperature were 5.8 and 25°C, respectively. A Pt counter electrode (Pt foil) and a silver/silver chloride reference electrode (Ag/AgCl, 3.5M) were used. Electrodeposited samples were rinsed under gentle flow of distilled water for a few seconds and ultrasonically cleaned in acetone for 1 minute.

2.2. Corrosion tests and surface observations

Corrosion tests were carried out in the Ringer's solution (8.6 g/L NaCl, 0.3 g/L KCl and 0.48 g/L CaCl$_2$) at 25°C. The pH was adjusted to 7.2 (by adding NaOH). An AUTOLAB potentiostat/ galvanostat and a classical three-electrode cell were used. Polarisation curves (1 mV/s) were plotted from -850 mV vs. Ag/AgCl up to ~ 300 mV vs. Ag/AgCl. No prior polarisation in the cathodic domain was performed.

Surface observations were performed using a field-emission scanning electron microscope (FE-SEM, JEOL 7600F) coupled with energy dispersive X-ray spectroscopy (EDS).

3. Results and discussion

3.1. Electrochemical measurements

Fig. 2(a)) shows the evolution of the current density vs time during electrodeposition of the two electrodes for 250 minutes. Solid lines represent experimental curves and dotted lines were obtained by extrapolating experimental data. For disk electrodes, the current density slightly increases (shift to negative values) over time, between -15 µA/cm^2 at the onset of electrodeposition and -19 µA/cm^2 for 250 minutes. This means that the growth rate is almost constant over time. Extrapolation of exprimental data indicates that the limiting current density is -32 µA/cm^2.

By contrast, for clamped wire electrodes, the current density first increases sharply to reach a value of about -121 µA/cm^2 after 2 minutes of electrodeposition (graph inset in Fig. 2(a)). This value is ~ 7.5 times greater than that mesured on disk electrodes. Then, the current density remains constant for several minutes (between 2 and 10 minutes of electrodeposition). From 10 minutes of electrodeposition, it starts to decrease (shift to
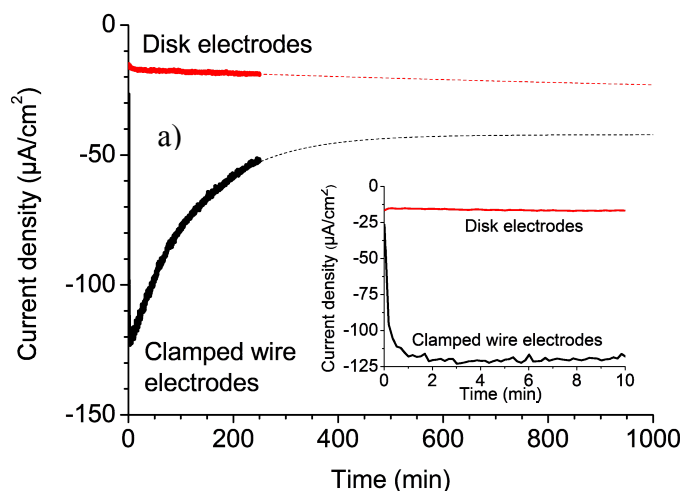

Fig. 2. Evolution of the current density vs. time during electrodeposition of the two types of electrodes (solid lines = experimental data and dotted lines = extrapolation)

positive values). Extrapolation of experimental data (dotted line in Fig. 2(a)) indicates that the limiting current density value is ~ -42 µA/cm^2. It is slightly greater than that estimated for disk electrodes (of about -32 µA/cm^2). Therefore, the growth rate is
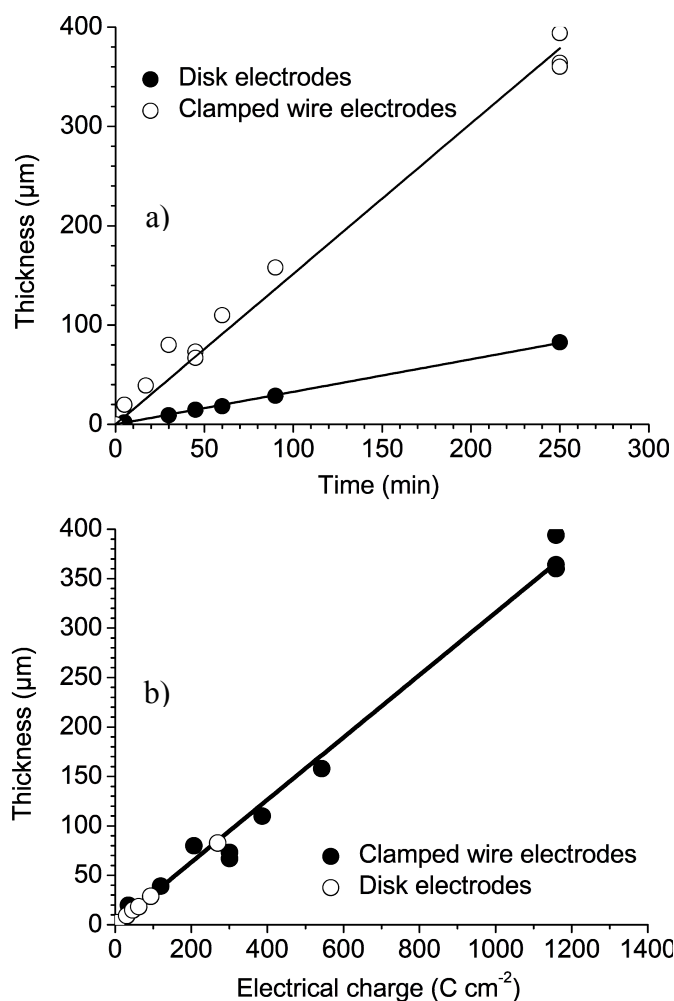

Fig. 3. Evolution of the coating thickness vs. (a) time and (b) electrical charge (absolute values)

faster on clamped wire electrodes than on disk electrodes. This was confirmed by plotting the coating thickness vs electrodeposition time, Fig. 3(a). A linear relatioship was found between thickness and time for the two electrodes. However, the difference of slope (corresponding to the rate growth) between the two staight lines is ~5 (1.5 µm/min for clamped wire lectrodes and 0.33 µm/min for disk electrodes).

These results show that the limiting current density value depends on the electrode geometry. Electrodeposition of Co-Mo/TiO$_2$ nano-composite coatings is then mass-transfer control. Planar diffusion is predoninant for disk electrodes. At the onset of electrodeposition (times less than 10 minutes), cylindrical diffusion operates for clamped wire electrodes. The limiting current density is larger with cylindrical diffusion than with planar diffusion, leading to higher current densities on clamped wire electrodes. As electrodeposition proceeds, the diameter of the clamped wire electrodes increases. It increases by roughly one order of magnitude, from 100 µm at the onset (diameter of the Co wire) up to 900 µm for 250 minutes (diameter of the coated wire after 250 minutes). The mass transport regime then evolves progressively from cylindrical diffusion at short times (times less than 10 minutes) to planar diffusion at long times (times greater than 10 minutes). The current density values at long times (estimated from extrapolation) are then very close for the two electrodes.

The coating thickness was found to be proportional to the electrical charge density (Fig. 3(b)) according to Faraday's law. The same relationship was found for both electrodes, indicating that the same reactional mechanisms occur on both electrodes. Only kinetics of reactions are affected by the electrode geometry (controlled by diffusion). In addition, the comparison of the physical-chemical propertie of coatings electrodeposited on both types of electrodes must be performed for a fixed value of the electrical charge density, and not for an electrodeposition time.

3.2. Microstructure of Co-Mo/TiO$_2$ nano-composite coatings

Top-view and cross-section FE-SEM/EDS observations were performed on Co-Mo/TiO$_2$ nano-composite coatings electrodeposited on both electrodes. For electrical charge density values less than ~60 C cm^{-2}, a nodular structure is observed for both electrodes (Fig. 4(a1-a2) for clamped wire electrodes and Fig. 4(b1-b2) for disk electrodes). Spherical nodules can be easily observed on top-view images (Fig. 4(a1) and 4(b1)). From cross-section images (Fig. 4(a2) and 4(b2)), it can also be seen that coatings are compact (no voids). In a previous study [1], it was shown that they are very beam sensitive. Cracks quickly
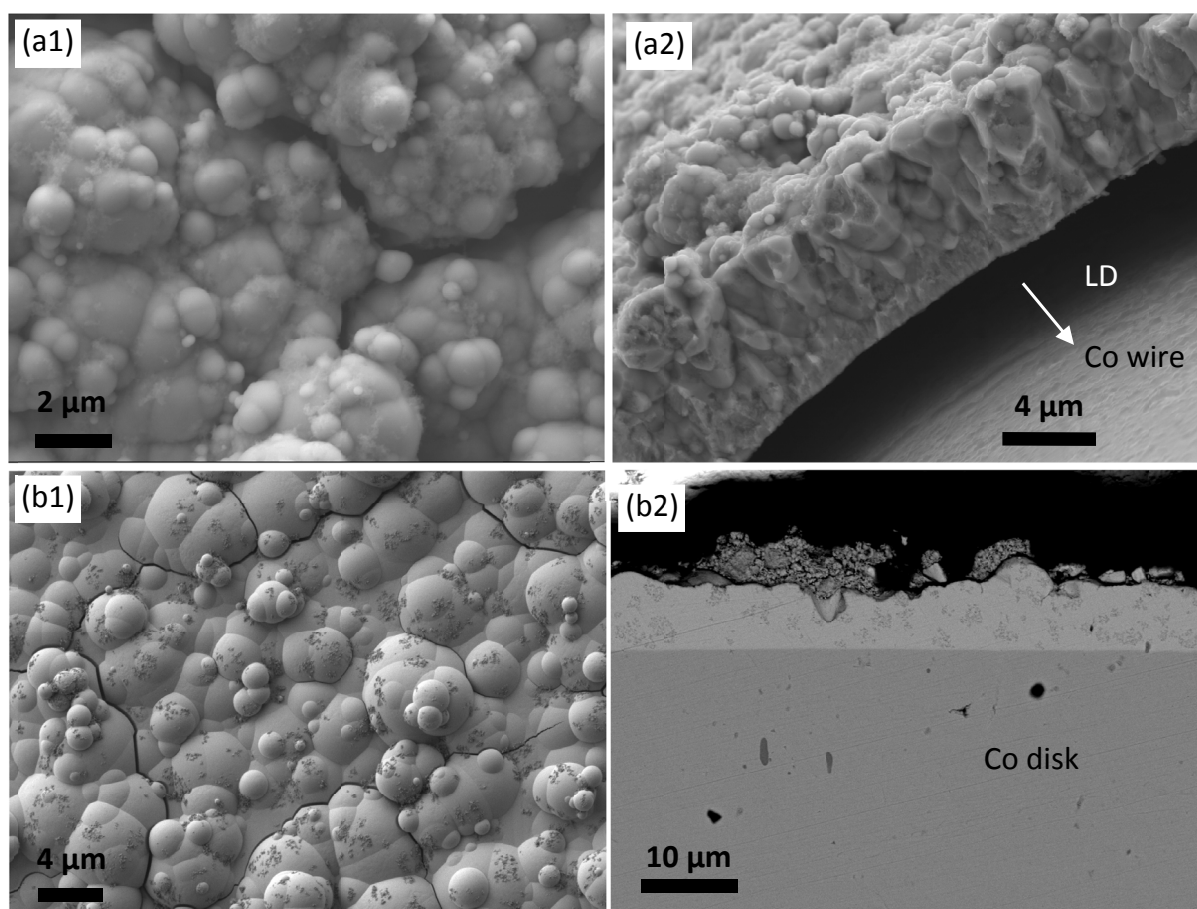

Fig. 4. FE-SEM images (1 = top-view and 2 = cross-section) of the coatings electrodeposited on (a) clamped wire electrode for 5 minutes (electrical charge density of 35 C cm^{-2}) and (b) disk electrode for 30 minutes (electrical charge density of 30.4 C cm^{-2}). LD = longitudinal direction
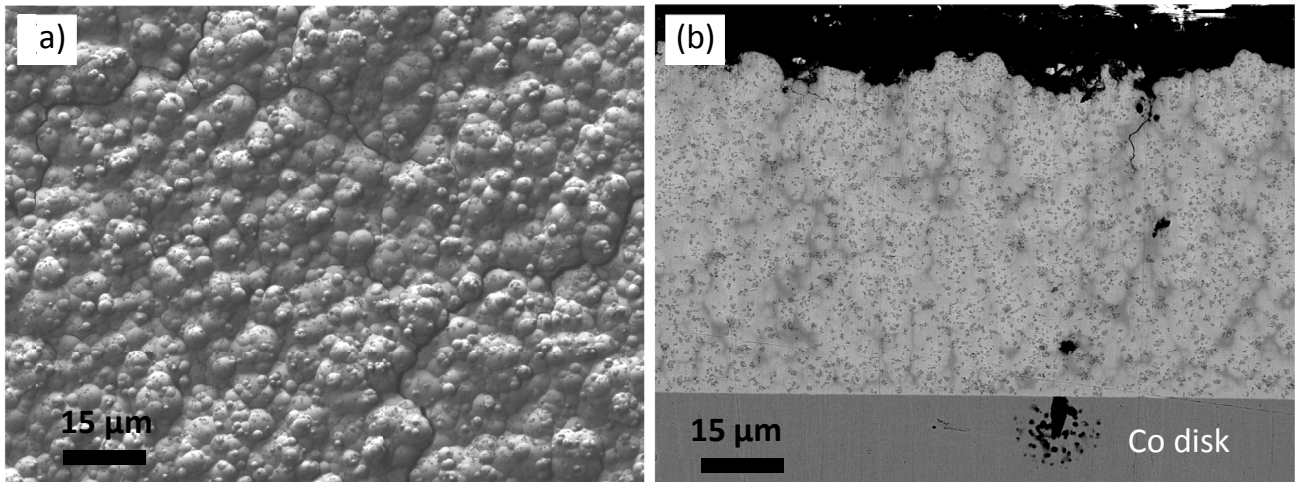
Fig. 5. (a-b) FE-SEM images of the coating electrodeposited on the disk electrode for 250 minutes (electrical charge density of 270 C cm^{-2})

appear upon exposure to the FE-SEM/EDS electron beam (as those visible in Fig. 4(b1) for example). No cracks were observed using atomic force microscopy (AFM) [1], but chemical analysis could not be performed.

For electrical charge density values greater than ~60 C cm^{-2}, all coatings on disk electrodes have a granular structure (Fig. 5(a-b)). Cross-section observations (Fig. 5(b)) show that they are again compact. They adhere very well to the substrate.
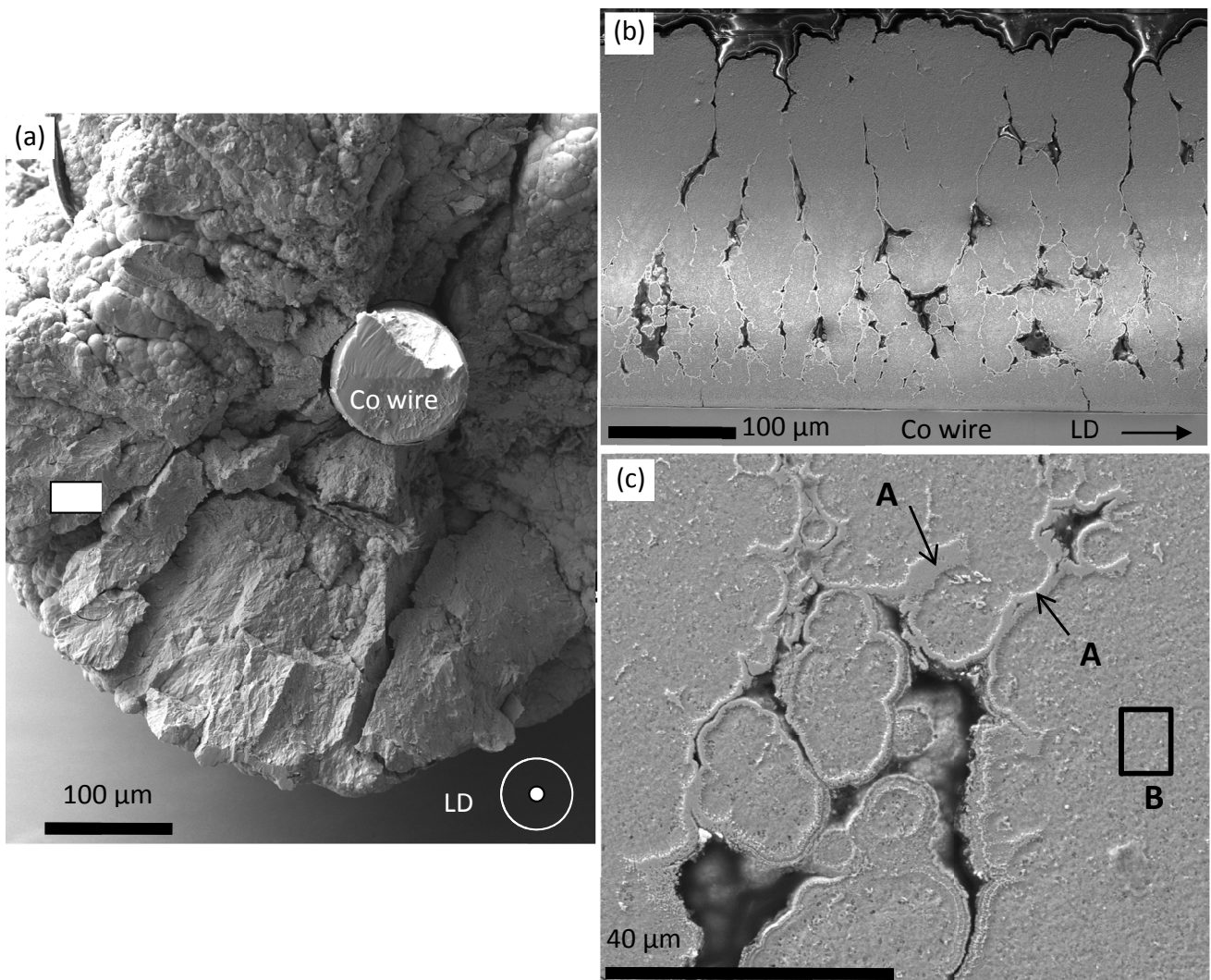

Fig. 6. (a-c) FE-SEM images of the coating electrodeposited on the clamped wire electrode for 250 minutes (electrical charge density of 1159 C cm^{-2}). LD = longitudinal direction

There is no micro-cracks or voids in the coatings an at the substrate / coating interface. FE-SEM/EDS analyses indicate that these coatings have heterogeneous composition. Dark zones in FE-SEM images are poorer in molybdenum (average values from several EDS analyses: 17.3±1.1 at.% C, 1.7±0.4 at.% O, 1.4±0.5 at.% Mo and 79.6±1.7 at.% Co). By contrast, bright zones contains (average values from several EDS analyses) 22.2±1.3 at.% C, 2.4±0.3 at.% O, 9.9±0.9 at.% Mo and 65.5±1.2 at.% Co. The transition between the nodular structure and the granular one during electrodeposition has recently been studied on disk electrodes [16]. It has been proposed that this transition is due to local diffusion fields induced by surface topography.

By contrast to the previous case (disk electrodes), all coatings formed on clamped wire electrodes for an electrical charge density greater than ~60 C cm^{-2} have a columnar structure (Fig. 6(a-c)). A high density of narrow and deep channels is visible on cross-section images. The electrolyte can flow in these channels, but it cannot be easily renewed. Therefore, during electrodeposition in the channels, Mo_4^{2-} ions are quickly consumed and only cobalt is deposited (zones A in Fig. 6(c)). In Zones A, EDS analyses give : 6.1±1 at.% C, 3.3±0.5 at.% Mo and 90.6±0.8 at.% Co. In Zone B EDS analysis gives: 10.2±1.5 at.% C, 4.5±0.4 at.% O, 12.6±1.2 at.% Mo, 1.2±0.2 at.% Ti and 71.4±1.3 at.% Co

3.3. Corrosion behaviour of coatings in Ringer's solution

Fig. 7 shows the polarisation curves in the ringer's solution at 25°C (aerated solution) of the Co-Mo nano-crystalline coatings formed on disk and clamped wire electrodes for 250 minutes. The two curves have the same shape, indicating that the two coatings have the same electrochemical behaviour. Region I corresponds to the cathodic domain. The main reaction is the oxygen reduction reaction (reaction 1):

$$O_2 + 2H_2O + 4e^- \rightarrow 4OH^- \qquad E^0 = 0.4 \text{ V vs. NHE} \qquad (1)$$

Region II corresponds to the oxidation of the coating [1] whereas Region III is mainly related to preferential dissolution of cobalt. In the three region is current density is slightly greater on the clamped wire electrode than on the disk electrode. This may be due to the presence of channels in which the electrolyte can flow. In this case, the surface area in contact with electrolyte is underestimated (the current density is overestimated). Therefore, these results show that both coatings have the same electrochemical behaviour and that the presence of channels in the coating formed on the clamped wire electrode has no significant influence on the electrochemical response.

4. Conclusions

It was shown that Co-Mo/TiO$_2$ nano-composite coatings can be electrodeposited on different electrode geometries. How-
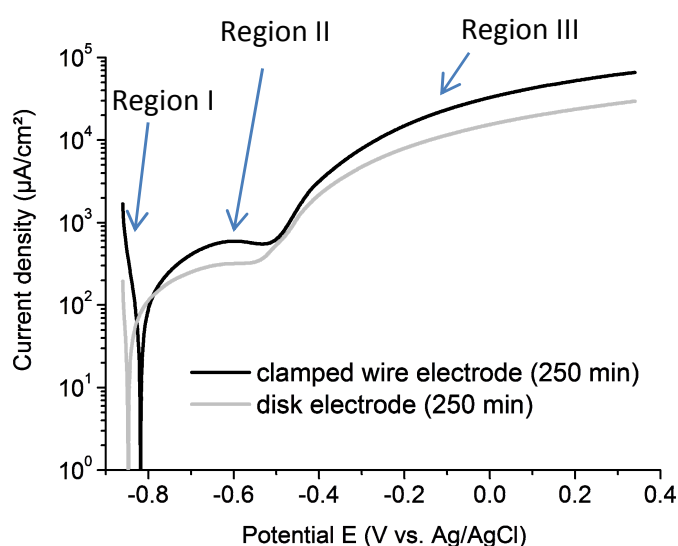

Fig. 7. Polarisation curves (1 mV/s) in the Ringer's solution at 25°C of the two coated electrodes

ever, the diffusion processes and the growth rate depend on the electrode geometry. The microstructure may then be different (numerous pores and channels are visible on the clamped wire electrode), but the corrosion behaviour is not affected by these differences.

REFERENCES

[1] H. Krawiec, V. Vignal, M. Latkiewicz, F. Herbst, Appli. Surf. Sci. **427** (7), 1124-1134 (2018).

[2] E. Gomez, E. Pellicer, X. Alcobé, J. Solid State Electrochem. **8** (7), 497-504 (2004).

[3] V.S. Kublanovskii, Y.S. Yapontseva, Y.N. Troshchenkov, V.A. Gromova, Russ. J. Appl. Chem. **83** (3), 440-444 (2010).

[4] Q.F. Zhou, L.Y. Lu, L.N. Yu, X.G. Xu, Y. Jiang, Electrochim. Acta **106**, 258-263 (2013).

[5] Y. Messaoudi, N. Fenineche, A. Guittoum, A. Azizi, G. Schmerber, A. Dinia, J. Mater. Sci.: Mater. Electron. **24** (8), 2962-2969 (2013).

[6] E. Gomez, E. Pellicer, E. Valles, J. Electroanal. Chem. **556**, 137-145 (2003).

[7] E. Pellicer, E. Gomez, E. Valles, Surf. Coat. Tech. **201** (6), 2351-2357 (2006).

[8] V.Q. Kinh, E. Chassaing, M. Saurat, Electrodepos. Surface Treat. **3** (3), 205-212 (1975).

[9] L. Anicai, S. Costovici, A. Cojocaru, A. Manea, T. Visan, Trans. IMF **93** (6), 302-312 (2015).

[10] E. Gomez, E. Pellicer, E. Vallés, Electrochem. Commun. **6** (8), 853-859 (2004).

[11] E. Gómez, E. Pellicer, E. Vallés, J. Electroanal. Chem. **568**, 29-36 (2004).

[12] E. Gómez, E. Pellicer, E. Vallés, J. Electroanal. Chem. **517**, 109-116 (2001).

[13] E. Gómez, E. Pellicer, E. Vallés, Surf. Coat. Tech. **197**, (2-3) 238-246 (2005).

[14] A. Subramania, A.R. Sathiya Priya, V.S. Muralidharan, Int. J. Hydrogen Energy **32** (14), 2843-2847 (2007).

[15] H. Krawiec, V. Vignal and M. Latkiewicz, Mater. Chem. Phys. **183**, 121-130 (2016).

[16] H. Krawiec, V. Vignal, A. Krystianiak, O. Heintz, M. Latkiewicz, Surf. Coat. Tech. Submitted.

[17] H. Krawiec, V. Vignal, A. Krystianiak, Y. Gaillard, S. Zimowski, Appl. Surf. Sci. **475**, 162-174 (2019).